Astron. Astrophys. 268, 736–748 (1993)

ASTRONOMY AND ASTROPHYSICS

Centre-to-limb variation of the Stokes V asymmetry in solar magnetic flux tubes

M. Bünte[1], S.K. Solanki[1], and O. Steiner[2]

[1] Institute of Astronomy, ETH-Zentrum, CH-8092 Zürich, Switzerland
[2] Kiepenheuer-Institut für Sonnenphysik, Schöneckstrasse 6, W-7800 Freiburg, Federal Republic of Germany

Received September 3, accepted October 3, 1992

Abstract. The centre-to-limb variation (CLV) of synthetic Stokes V line profiles of the spectral lines Fe I 5250.22 Å and Fe I 5083.35 Å is computed and compared with observations. The basic elements of the hydromagnetic model used to calculate the Stokes V profiles consist of a vertical cylindrical flux tube surrounded by a field-free plasma in stationary motion with a downflow along the tube boundary and an upflow further away from it. It is shown that an array of such magnetic flux tubes reproduces the peculiar observed centre-to-limb variation of the Stokes V asymmetry, in particular the sign reversal of the asymmetry near the limb (at $\mu \simeq 0.4$ for Fe I 5250.22 Å). We determine a minimum number of model components needed for the reproduction of the Stokes V area asymmetry and study the influence of various free model parameters thereon. Satisfactory agreement between synthetic and observed Stokes V profiles can only be achieved by including a considerable amount of realism into the model such as a granular temperature-velocity correlation. This suggests that the basic picture of magnetic structures in the quiet solar network and active region plages is correct. The variation of the Stokes V asymmetry has the potential to serve as a sensitive diagnostic of convection in active regions. This is corroborated by the great sensitivity of the area asymmetry of Fe I 5083.35 Å line to details of the model.

Key words: Sun: magnetic fields – magnetic flux tubes – Sun: photosphere – Sun: active regions – Sun: granulation – line profiles – polarization

1. Introduction

Although much of the photospheric magnetic fine structure can still not be spatially resolved by observations, it can be studied indirectly through the spectro-polarimetric signature of the Zeeman effect on atomic lines formed in photospheric magnetic fields. In this context the directly observable Stokes parameters I, Q, U, and V of a spectral line have proved to be a powerful tool in deriving semi-empirical models of photospheric magnetic elements in plages and the network (see reviews by Solanki 1992; Stenflo 1989). Such investigations have led to the view that the photospheric magnetic field in the quiet solar network and in active region plages is concentrated into kilo Gauss flux tubes that are located in the dark and downflowing intergranular spaces as a consequence of flux expulsion (see, e.g., Schüssler 1990). Although the individual flux tubes are surrounded by downflowing gas, there is no sizeable downflow within them. In the photospheric layers flux tubes spread rapidly with increasing height due to the exponentially decreasing gas pressure until they merge and fill almost the entire atmosphere above the merging height. As a consequence the magnetic field strength of the tube decreases with height.

One remarkable feature of Stokes V profiles observed in active region plages and the quiet solar network is their pronounced asymmetry (Stenflo et al., 1984; Wiehr 1985). Near disc centre the area and amplitude of the blue wing of Stokes V of almost all unblended lines exceed those of the red wing by several percent (Solanki & Stenflo 1984, 1985), i.e., $\delta A = (A_b - A_r)/(A_b + A_r) > 0$ and $\delta a = (a_b - a_r)/(a_b + a_r) > 0$, where A_b, A_r denote the areas, a_b, a_r the amplitudes of the blue and red wing, respectively. For LTE, Auer & Heasley (1978) have shown that the area asymmetry can only be explained in terms of velocity gradients. The first mechanism based on velocity gradients was proposed by Illing et al. (1975) and relied on the overlap of gradients in magnetic field strength and velocity. However, if we accept the current basic picture outlined above, in particular that the field strength decreases with height, then, as shown by Solanki & Pahlke (1988), a stationary flow which gives the correct Stokes V within the magnetic flux tube implies a shift of the zero-crossing wavelength of the Stokes V profile larger than the observed upper limit of $\pm 250\,\mathrm{m\,s^{-1}}$ (Stenflo & Harvey 1985; Solanki 1986; Stenflo et al., 1987; Wiehr 1987; Solanki & Pahlke 1988). Other combinations of overlapping magnetic and velocity gradients have been proposed which can also produce asymmetric Stokes V profiles with only small zero-crossing shifts (Sánchez Almeida et al. 1988, 1989). However, such combinations invariably contradict the basic picture outlined above, since they require the field strength to increase

Send offprint requests to: M. Bünte

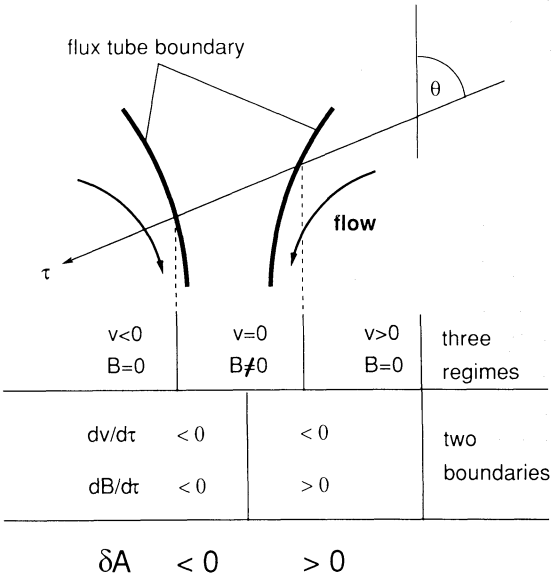

Fig. 1. Schematic illustration of the longitudinal gradients of the magnetic and velocity fields along a highly inclined ray passing through a flux tube. According to Eq. (1) the contributions to the Stokes V asymmetry from the two intersections of the ray with the flux-tube boundary counteract. Note that $B = |\boldsymbol{B}|$, whereas v is the line-of-sight velocity (positive in the direction of increasing optical depth τ)

with height (or, more exactly, with decreasing optical depth). Van Ballegooijen (1985) pointed out that plasma flows in the *non-magnetic surroundings* of the flux tubes may also produce asymmetric Stokes V profiles. Grossmann–Doerth et al. (1988, 1989) then showed that if the velocity and the magnetic field are spatially separated, as proposed by Van Ballegooijen (1985), asymmetric, but unshifted, Stokes V profiles are produced.

Solanki & Pahlke (1988) have shown that the sign of the Stokes V area asymmetry depends on the signs of the longitudinal gradients of the magnetic and the velocity field alone:

$$\frac{d|\mathbf{B}|}{d\tau}\,\frac{dv(\tau)}{d\tau} \quad \begin{cases} < 0 \implies \delta A > 0\,, \\ > 0 \implies \delta A < 0\,. \end{cases} \tag{1}$$

Only the absolute value of the magnetic field is of importance, not its polarity, whereas the sign of the velocity plays a vital role. At solar disc centre in the standard picture of expanding flux tubes, rays parallel to the observer's line of sight only pass from the magnetic into the non-magnetic atmosphere if traveling in the direction of increasing optical depth, but not the other way round. Closer to the limb, however, a particular ray may cross the border between magnetic and non-magnetic regimes in both directions. Such a case is schematically illustrated in Fig. 1. In a symmetric velocity field, directed towards the flux-tube axis, the Stokes V asymmetries produced at the two boundaries will, in general[1], be of opposite sign. It is therefore not obvious whether the basic picture can account for the change in sign of the area asymmetry near the limb observed for Fe I 5250.22 Å by Stenflo et al. (1987) and for a larger sample of spectral lines by Pantellini et al. (1988). The aim of the present study is to find out under what conditions the area asymmetry changes sign near the limb. We also aim to obtain an idea of the diagnostic potential of the centre-to-limb variation (CLV) of δA. In the present investigation we restrict our attention to the *area* asymmetry δA since the mechanism for its production at disc centre is well understood. The *amplitude* asymmetry δa, in contrast, may be produced or changed by a much larger variety of causes (e.g. velocity changes along the line of sight, perpendicular to it, or in time, macroturbulence, etc.), so that its production, even at disc centre, is still partially unclear (compare Grossmann-Doerth et al. 1991 with Degenhardt & Kneer 1992). In any case, we think that the correct reproduction of the area asymmetry is a more stringent test for the basic model than the reproduction of the amplitude asymmetry would be. A preliminary version of some of the results presented here is to be found in Bünte et al. (1991).

[1] The velocity field must have sufficiently strong horizontal components for this to be valid.

2. The standard model

The model we adopt for active region plages and the quiet solar network is stationary, i.e., time independent. It consists of a cluster of rotationally symmetric, vertical flux tubes in magnetohydrostatic equilibrium. In accordance with the observations of Solanki (1986), we suppress any stationary velocity inside the tubes. Instead, we assume each flux tube to be surrounded by field-free (non-magnetic) plasma in stationary motion, with a downward directed flow as shown in Fig. 2. At the photospheric level, $\tau_{5000} = 1$, the flux tubes have a magnetic field strength of about 1600 G and are interspersed in the non-magnetic plasma with a filling factor of 5 to 25 %. In the following we describe in detail the magnetic field structure, the velocity field, and the temperature structure of the standard model with which most of the calculations presented in Sects. 4 and 5 have been carried out. In order to isolate the effects of the various components of the standard model on the Stokes V profiles, we also make use of simpler versions of the standard model in Sect. 4 which will be described there.

2.1. Magnetohydrostatic field structure

The basic element of the model is a vertical, rotationally symmetric magnetic flux tube embedded in a external, field-free medium. The plasma is assumed to be infinitely conducting, so that the magnetic field is separated from the surroundings by a vanishingly thin current sheet. The location of the current sheet is determined by the prescribed gas pressure difference between the external medium and the flux tube, or internal, atmosphere. The magnetic fields of all flux tubes considered here are untwisted. For the computation of the field structure we use the code developed by Steiner et al. (1986) which is based on an iterative solution procedure for the Grad-Shafranov equation.

The second component of our model is the external, non-magnetic fluid in stationary motion. Its velocity field is described in more detail in the following subsection. Here we

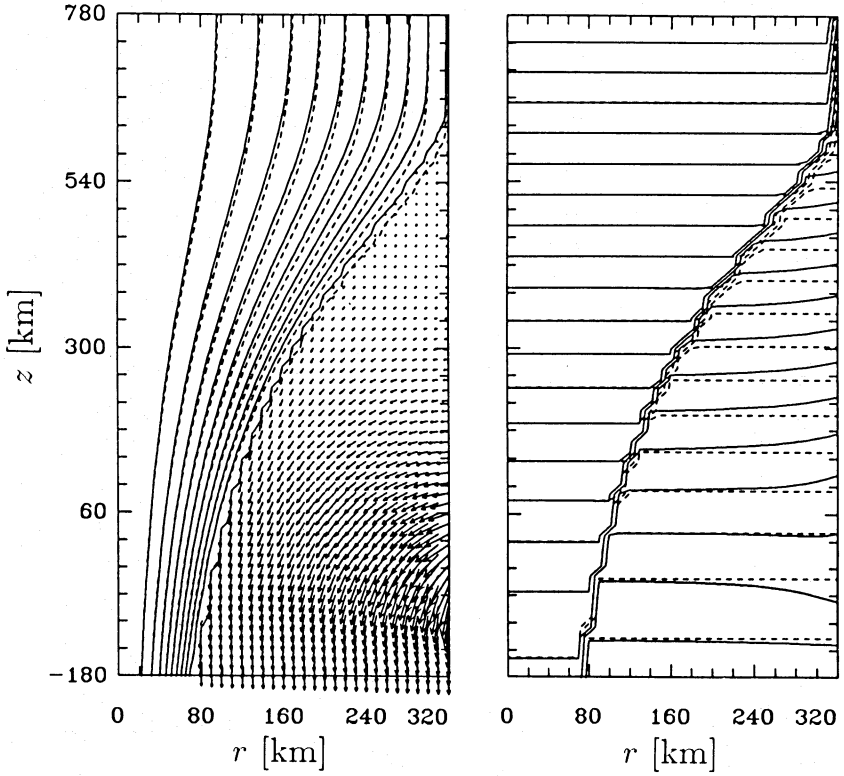

Fig. 2. Left: Rotationally symmetric magnetic flux tube in magnetohydrostatic equilibrium ($B(r = 0, z = 0) = 1600$ G) surrounded by a field-free downdrafting plasma ($v_{\max} = 6$ km/s). Only one half of the tube is shown. Dashed field lines result in the absence of the external flow. Right: corresponding isobars calculated under the assumption of horizontal temperature equilibrium from Eqs. (3) and (4). Apart from the discontinuity at the flux-tube boundary any radial variation of the gas pressure arises from the external flow. Again, dashed lines result if the external flow field is omitted

briefly discuss the interaction of this stationary flow with the magnetic field.

Since the medium is assumed to be infinitely conducting the magnetic field is "frozen" into the plasma. Consequently, the current sheet of the flux tube forms a flexible boundary for the external flow, i.e., a boundary which cannot be crossed but may be deformed by the plasma motion. Stationarity requires $\boldsymbol{n} \cdot \boldsymbol{v} = 0$ at every point along this boundary (where $\boldsymbol{v}$ is the velocity vector and $\boldsymbol{n}$ is the normal to the flux-tube boundary) and the condition for pressure equilibrium is unchanged compared to the static case:

$$p_i + \frac{B^2}{8\pi} = p_e \ , \tag{2}$$

where $p_{i,e}$ are the gas pressure in the internal and the external atmosphere, respectively. The flow field therefore influences the magnetic field solely through its effect on the external gas pressure, p_e.

A rough estimate of the resulting change in p_e and hence of the magnetic field structure can be obtained as follows. In the photospheric layers of the atmosphere, the internal magnetic pressure and the external gas pressure are comparable in magnitude, i.e., $B^2 \simeq 8\pi p_e$. If the flow velocities are small compared to the adiabatic sound speed, viz. $v^2/C_s^2 = 2p_{\rm dyn}/(\gamma p_{\rm gas}) \ll 1$, the dynamic pressure is small compared to both gas pressure and magnetic pressure $B^2/(8\pi)$, leading to only slight changes in the magnetic field structure. In the photosphere where typical flow speeds are of the order of 10^5 cm/s $\approx C_s/10$ this approximation seems to be justified.

In order to obtain a quantitative estimate we iterate the computation of the magnetic field by calculating the external flow field at the end of each iteration step using the actual current sheet as a *fixed boundary*. The new external pressure in function of radius and height can be obtained from an integral of the equation of motion:

$$p_e(r,z) = p_e(r,0) \exp\left[- \int_0^z \mathrm{d}z' \left(\frac{1}{H(z')} + \frac{1}{H^*(r,z')} \right) \right] \ , \tag{3}$$

where $H(z) = \mathscr{R}T(z)/(\bar{\mu}g)$ is the local pressure scale height which – under the assumption of radially constant temperature and chemical composition – is a function of z alone ($\mathscr{R}$ is the gas constant, T is the gas temperature, $\bar{\mu}$ is the mean relative molecular weight, and g is the gravitational acceleration). H^* is given by

$$\frac{1}{H^*(r,z)} = \frac{\bar{\mu}}{\mathscr{R}T(z)} \left(v_r \frac{\partial v_z}{\partial r} + v_z \frac{\partial v_z}{\partial z} \right) \ , \tag{4}$$

with an external velocity field $\mathbf{v} = v_r \mathbf{e}_r + v_z \mathbf{e}_z$. The magnitude of $1/H^*$ depends on the spatial gradients of the velocity field.

The new external pressure stratification is then used for the calculation of the new magnetic field. Convergence is obtained after a few iterations. Figure 2 shows the resulting magnetic field lines and isobars (solid lines) together with the respective results in the absence of an external flow (dashed lines). Obviously the differences are small, in particular for the magnetic field and the atmospheric structure close to the tube boundary, i.e. in that region which is of most importance for the asymmetry of the Stokes V signal. Therefore, in all the following models we have calculated the magnetic field and the external flow separately, thereby simplifying the numerical procedure considerably.

2.2. *The external velocity field*

In the adopted standard model the individual flux tubes are surrounded by downflowing gas, although there is no motion within them. Such external downflows have previously been proposed to reconcile the red shifted Stokes I profiles with their corresponding unshifted Stokes V zero-crossing wavelength (Stenflo, 1976). Title et al. (1987) find a correlation between small-scale magnetic flux concentrations, downdrafts, and dark intergranular lanes, suggesting small scale magnetic flux tubes to be located within downdrafting intergranular regions. So far there are no direct observations of downflows in the close vicinity of magnetic elements, simply because of the limited spatial resolution of direct observations.

From a theoretical point of view the location of magnetic flux tubes in intergranular downdrafts is a natural outcome of the flux expulsion process by which the magnetic flux concentrations are thought to form (see, e.g., Schüssler 1992; Steiner 1992). Deinzer et al. (1984) and Knölker et al. (1991) find by numerical simulation that the mere existence of an intense magnetic flux concentration leads to a rapid downflow of up to 6 km/s in the close vicinity of the magnetic flux boundary. This persisting mass flow is a result of photospheric magnetic flux tubes acting as heat leaks: the non-magnetic material adjacent to the tube is subject to radiation losses into the evacuated tube thereby cooling off, descending, and being replenished by horizontally inflowing hot plasma. Nordlund (1986) reports on 3-D MHD simulations showing stagnant regions of magnetic flux concentrations surrounded by downward directed mass motion.

To keep the numerical procedure simple we have chosen potential velocity fields, of which Fig. 4 gives an example. It shows a narrow strong downflow in the close vicinity of the magnetic field concentration, which is fed by a broad upflow and a horizontal flow further away. This velocity field is computed in cylindrical geometry. Since it is impossible to mimic the overturning of convective motions with a single velocity potential, we use a piecewise potential velocity field consisting of a potential downflow, $\mathbf{v}_d = \nabla\Phi_d$, in the immediate surroundings of the flux tube connected to a potential upflow, $\mathbf{v}_u = \nabla\Phi_u$, at some distance from the flux-tube boundary. The respective velocity potentials, $\Phi_{u,d}$, are determined by the equation of continuity, which, for given density stratification, poses a non-separable elliptic boundary value problem

$$\rho\Delta\Phi_{u,d} + \nabla\rho\cdot\nabla\Phi_{u,d} = 0\ . \tag{5}$$

The boundary condition at the interface of the two potential flow fields, i.e., the radial velocity there, must be prescribed. It is equal at both sides of the interface, and since the density is equal as well, this prescription guarantees mass conservation in the whole computational domain. In addition, the velocity field is continuous everywhere, but not differentiable at the interface of the two potential fields. The interface is located at radial distance R_i from the flux-tube axis.

At the lower boundary of the two adjacent computational domains we demand the radial velocity component to vanish. At all other boundaries except for the intermediate one we require tangential motions, i.e., $\nabla_{\mathbf{n}}\Phi = 0$, where $\mathbf{n}$ is the normal to the respective boundary and Φ is the respective velocity potential. In particular, this guarantees that no mass transfer can occur across the flux-tube boundary. Since the shape of the flux-tube boundary is curved, it is convenient to use a body fitted grid for the computation of the downflow field. Equation (5), then, is solved in a rectangular cartesian coordinate system and the result is transformed back into the coordinate system of Fig. 4 for the diagnostic procedure. The details of this computational procedure can be found in Bünte (1989).

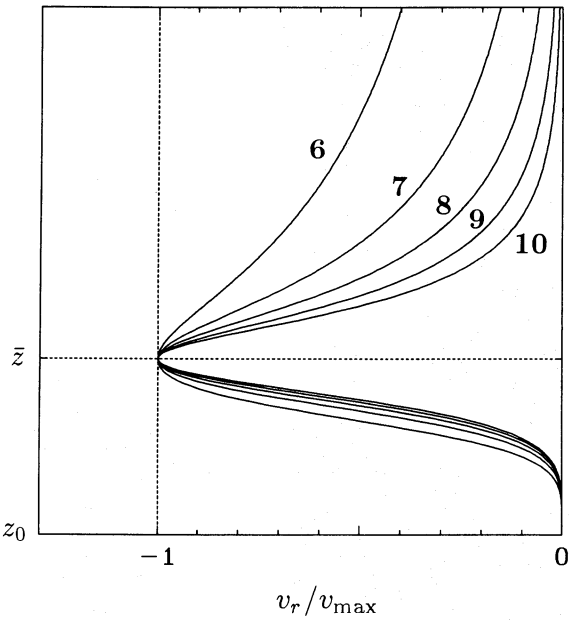

Fig. 3. Normalized radial velocity profiles calculated from Eq. (6) for $m = 5$ and labeled with various values of n. Further prescribed parameters are the maximum radial velocity, $v_{\max}$, the height, $\bar{z}$, at which $v_r = -v_{\max}$, and Z_0, the base of the computational box

We are left with prescribing the radial velocity profile as a function of height along the interface of the upflow and the downflow region. For this purpose we have chosen the following parametrization which mimics the radial velocity profile in granules obtained from self-consistent granular models, such as those of Steffen et al. (1989):

$$v_r(z) = -v_{\max}\frac{(1+\beta)\zeta^m(z)}{1+\beta\zeta^n(z)}\ , \qquad \text{with} \quad \zeta(z) = \frac{z-Z_0}{\bar{z}-Z_0}\ , \tag{6}$$

where $\beta = m/(n-m)$ and $n > m$. Z_0 is the lower z-coordinate of the computational domain, $\bar{z}$ is the height at which the absolute value of the radial velocity, v_r, assumes its maximal value, $v_{\max}$. Finally, m and n are two exponents (not necessarily integer values), which determine the shape of the velocity profile. $v_r(z)/v_{\max}$ has been plotted in Fig. 3 for fixed $m = 5$ and various values of n.

There are five parameters which determine the external piecewise potential flow field: $v_{\max}$, the radial location, R_i, of the interface, the height $\bar{z}$ of the maximum radial velocity at

$r = R_i$, and the exponents m and n. For the starting point (origin) of the parametric survey presented in Sect. 5 we take the values $v_{\max} = 3$ km/s, $R_i = R_0 + 120$ km, $\bar{z} = 0$ km, $m = 5$, and $n = 9$. The flux tube has a radius of $R_0 = 100$ km at $\tau_{5000} = 1$ and expands with height until it merges with neighbouring tubes at a diameter of 900 km, corresponding to a filling factor of 5%. Here and in the following $z = 0$ corresponds to the geometrical height at which the optical depth, τ_{5000}, at vertical incidence reaches unity in the atmosphere surrounding the flux tube if its structure is that of the modified HSRASP model atmosphere defined below. The interface of the upflow and downflow region was placed at $R_i = 220$ km from the axis of symmetry of the magnetic flux tube. The choice of R_i depends on the criteria under which the model is to be compared with other models. In such comparisons either $(R_i - R_0)$ or the ratio of the radial extent of the upflow and the downflow region are kept constant. In any case, different spatial extents of the upflowing and downflowing parts of "granules" can be taken into account. The magnetic-field structure and the velocity field of the original standard model are shown in Fig. 4, left. A shortcoming of the present model remains the axially symmetric nature of the velocity field, that can be at best a crude approximation to a realistic three dimensional granular flow in the vicinity of a flux tube.

2.3. The temperature structure

In the entire volume we prescribe gas temperature, pressure, and density. For the magnetic interior we use the plage model of Solanki (1986). For the non-magnetic close surroundings we adopt a quiet sun model with a temperature profile similar to the HSRASP model of Chapman (1979) – the HSRA model of Gingerich et al. (1971) connected to the convection zone model of Spruit (1974) – but systematically cooler by 300 K. This temperature profile was found to provide the best fit to the observed δA values of four spectral lines at disc centre (Solanki 1989). At disc centre, only the close surroundings of the flux tube influence the formation of Stokes V profiles, since in this case the relevant lines of sight passing from the magnetic into the non-magnetic region never lie far from the flux-tube surface over the height range of the spectral line formation. In general this is not true for inclined lines of sight (see also Sect. 3.1). Consequently we also have to specify the atmosphere in the wider surroundings of the flux tube.

We adopt the following temperature structure for the region outside the flux tubes:

$$T(z) = \begin{cases} T^*_{\mathrm{HSRASP}}(z)\,, & \text{in downflows,} \\ T^*_{\mathrm{HSRASP}}(z) + \dfrac{v_z}{v_{z\,\max}}\Delta T\,, & \text{in upflows,} \end{cases} \tag{7}$$

where $v_{z\,\max}$ is the maximum upflow velocity (typically ≈ 3.8 km/s) and $T^*_{\mathrm{HSRASP}}(z) = T_{\mathrm{HSRASP}} - 300$ K. This choice implies a correlation between temperature and velocity similar to that seen in granulation: A warm, broad granular upflow and a cool rapid intergranular downflow. For ΔT we have chosen values of typically 500–1000 K for consistency with the 3-D model calculations of Nordlund (1985) and the most recent 2-D results of Steffen (1990).

3. Calculation of synthetic Stokes V profiles: radiative transfer along multiple rays

The computation of the hydromagnetics described in the previous section is followed by a *diagnostic procedure* which serves to determine the spectral signature of the model, i.e., the values of the emergent Stokes parameters of a given spectral line. In the present paper we are only interested in Stokes V. The diagnostics involve two steps: Firstly, the positioning of lines of sight (rays) across the hydromagnetic model and, secondly, the integration of the spectral line transfer equation for polarized light (Unno-Rachkovsky equation) along them.

3.1. Positioning of the lines of sight and the range of spectral line formation

First, the atmospheric quantities must be determined along a number of rays parallel to the line of sight passing at an angle θ to the vertical through the model. Only the line profiles averaged over all rays are finally compared with the spatially unresolved observations. We call this averaging over a number of rays a 1.5-D radiative transfer. Figure 4 shows the central cross section through a standard model tube and its immediate surroundings (left). The right panel shows a bundle of 20 parallel rays entering the model from the top at an angle of 70° to the vertical. Once a ray leaves the model to the left it re-enters it from the right at the same height. This corresponds to observing an array of identical flux tubes. The dots mark the points of support used for the radiative transfer calculations and must be chosen carefully. They are chosen such that the logarithm of the continuum optical depth τ_c is sampled at reasonable intervals. This is done as follows: starting at the top of the model atmosphere, at $z = z_1$ say, with a value of typically $\log \tau_1 = -7$, we use the gas pressure, density ρ_1, and temperature values there to calculate the electron pressure and absorption coefficient per unit mass κ_1 using the code by Gustafsson (1973). This is the first point along the ray. We now assume the next point to be located at a distance Δs "further down" the ray, i.e., at a height $z_2 = z_1 - \Delta s \cos\theta$, where we use the new gas pressure, new density ρ_2, and new temperature to determine the new electron pressure and absorption coefficient κ_2. Only now we can check at what optical depth τ_2 this new point lies using the trapezoidal formula:

$$\tau_2 = \tau_1 + \frac{\kappa_1\rho_1 + \kappa_2\rho_2}{2}\Delta s\,. \tag{8}$$

If $\Delta \log \tau_c \equiv \log \tau_2 - \log \tau_1$ exceeds a prescribed upper limit (typically 0.1) or is smaller than a lower limit (typically 0.01), we go back to the previous point (here point 1) and repeat the procedure using a smaller or larger spatial stepsize Δs, respectively.

In this manner point after point is added along the line of sight such that $0.01 \leq \Delta \log \tau_c \leq 0.1$ between two successive points until a value of $\log \tau_c \approx 1$ is reached. Within these limits

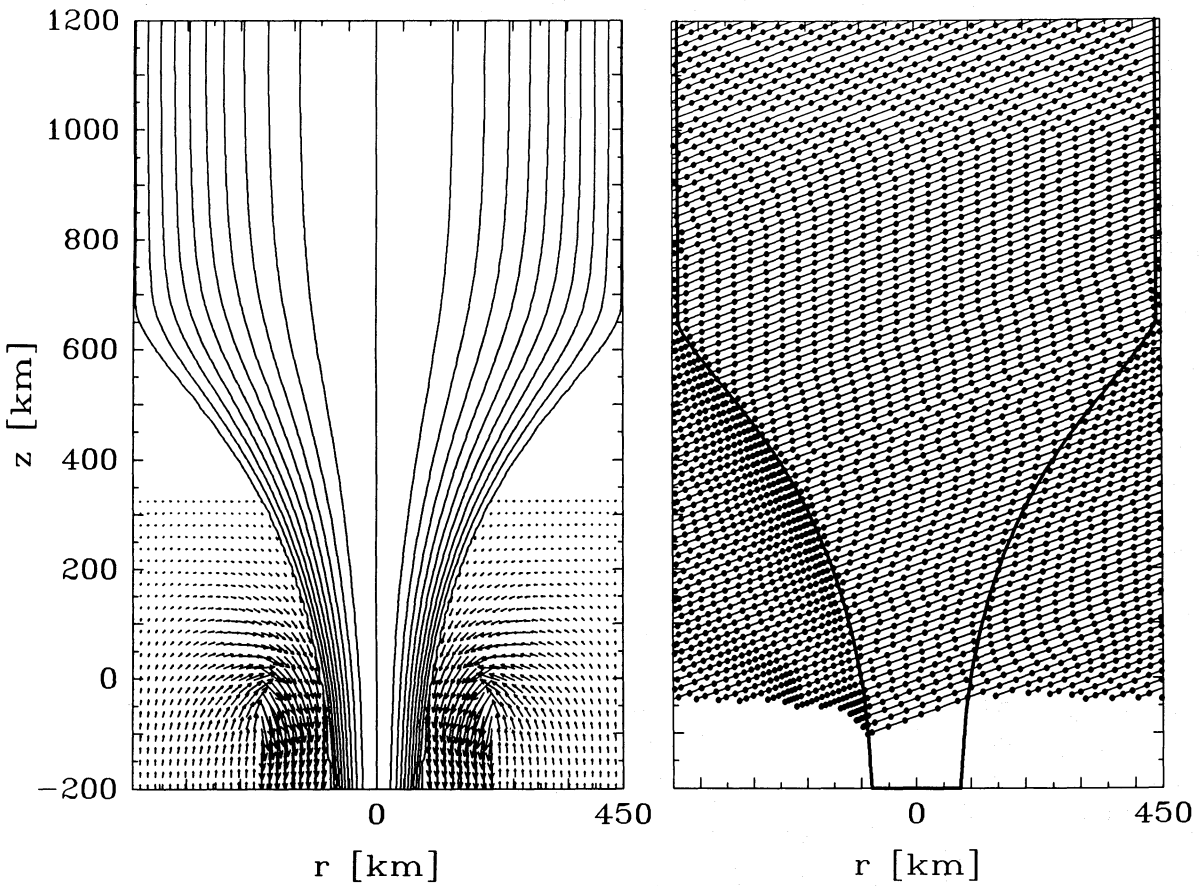

Fig. 4. Left: Cross section through the standard model: a vertical, rotationally symmetric magnetic flux tube in magnetohydrostatic equilibrium surrounded by a field-free plasma in stationary motion. Representative lines of force of the magnetic field are shown together with the velocity field (arrows). The velocity field is composed of two potential fields with the vertical velocity component being discontinuous at the radius where the two potential fields are matched (R_i = 220km). The tube has a magnetic field strength of 1600 G, a diameter of 200 km and a filling factor of 5 %. All these values refer to z = 0, at which height τ_{5000} = 1 in the field-free atmosphere. Maximum flow velocities are $\approx$ 4 km/s. Right: a bundle of 20 rays entering the model from the top at an angle of 70° to the vertical. Once a ray hits the left boundary of the frame it enters the model again from the right at the same height to simulate an array of neighbouring flux tubes. Along each ray the grid points (dots) for the radiative transfer calculations are chosen such that $0.01 \leq \Delta \log \tau_c \leq 0.1$. Note that apart from the drastic jump in density and temperature at the tube boundary also the temperature-velocity correlation in the external flow field [Eq. (7)] requires such an adaptive stepsize method to ensure good resolution

the stepsize is chosen such that each ray segment in the interior of a flux tube contains a sufficient number of grid points (ideally at least 10). This adaptive step size procedure allows us to resolve those regions along the line of sight where the spatial variation of the optical depth is high, e.g. at the boundaries between magnetic and non-magnetic plasmas.

The periodic arrangement of magnetic flux tubes is an important aspect of our calculations, since close to the limb a ray may pass through more than a single flux tube. This situation is depicted in more detail in Fig. 5. Figure 5a shows an array of magnetic flux tubes from above. In reality, of course, flux tubes lose their identity as they merge, in particular the rotational symmetry breaks down and the field should also fill the gaps between the circles in Fig. 5a. However, the spectral lines under consideration (Fe I 5250.22 Å and 5083.35 Å) are formed in layers well below the height at which merging occurs, so that the topological details of merging fields do not have any influence on the shape of these lines. A set of parallel planes, one of which contains the symmetry axes of the tubes, are chosen (indicated by the horizontal parallel lines in Fig. 5a). Each of the dots on these lines is the upper entrance point of a ray which lies in the corresponding plane and forms an angle θ with the vertical direction. Since we are only interested in Stokes V, which is not sensitive to the azimuthal angle of the field, it is sufficient to pierce only half of the rightmost thick circle in Fig. 5a with rays.

Figure 5b shows sets of rays lying within three different vertical planes of the model, indicated in Fig. 5a by the heavy horizontal lines. Since the model is defined only within the cylinder with a diameter to which the flux tube maximally expands, there are gaps in the vertical sections (with the exception of the one which contains the symmetry axis of the tubes) for which the atmospheric structure has yet to be defined. These gaps are filled by the field free atmosphere as defined at maximum radius. The

code used to place the rays and evaluate the atmospheric data along them is a modified and extended version of the one described by Ringenbach (1987) and De Martino (1986). For the current work typically 10×19 rays are laid through the model. Thus the complete Unno-Rachkovsky transfer equations must be solved along 190 rays to obtain the final Stokes V at a single wavelength point and a single position, i.e., θ value, on the solar disc.

We wish to emphasize two points: Firstly, although at solar disc centre the absolute horizontal scale of a thin flux tube has no influence on Stokes V, this is no longer the case when it is viewed at some aspect angle $\theta > 0$, as pointed out earlier by Walton (1987), Zayer et al. (1989), and Audic (1991). This is the reason why we consider the flux tube radius and the absolute sizes of the upflowing and downflowing components of the field-free atmosphere to be important free parameters. Secondly, near the limb the Stokes V profiles sample, or are sensitive to, a much larger fraction of the non-magnetic atmosphere than at disc centre. This is schematically indicated by the horizontal lines below the top frame of Fig. 5b. They indicate the horizontal range around a particular tube to which the Stokes V profile of a line formed between $\log \tau_c = -1$ and $\log \tau_c = -3$ is sensitive at solar disc centre (short line, on the right) and near the limb at $\theta = 70°$ (long line, to the left). Therefore, although at disc centre δA is determined by velocities close to the flux-tube boundary, at large θ, velocities far away from any flux tube also influence δA.

3.2. The integration of the line-transfer equation

The Stokes parameters for a particular spectral line are calculated numerically in LTE along each ray using a code based on the one described by Beckers (1969 a,b). For more details, see Solanki (1987). Finally, all the calculated profiles are added together. The resulting Stokes V profiles can be directly compared with observations having a low spatial resolution (an arc sec or worse). To determine the centre-to-limb variation of δA we calculate Stokes V for 9 different viewing angles, $\theta =$ 0°, 37.0°, 53.0°, 60.0°, 63.3°, 66.0°, 72.5°, 78.5°, 81.4°, corresponding to $\mu = 1.0$, 0.8, 0.6, 0.5, 0.45, 0.4, 0.3, 0.2, 0.15. We do not calculate Stokes profiles closer to the limb because, firstly, no reliable data are available for $\mu < 0.15$ and, secondly, at increasingly flatter incidence any given ray parallel to the line-of-sight passes through an ever larger number of flux tubes. This number increases very rapidly close to the limb. Since each additional flux tube introduces two new boundaries, a stable solution of the radiative transfer can only be obtained at the cost of introducing additional depth points, as described earlier in this section. This soon makes the cost of computing such profiles prohibitive. Finally, very close to the limb the effects of the curvature of the solar surface would have to be taken into account.

Audic (1991) has previously calculated spectral lines in a similar geometry. Our approach differs from his in that he considers only a single flux tube and simulates very high spatial resolution observations (with a beam of circular cross-section and diameter of $0.3''$) without a flow field, while we simulate low spatial resolution observations using a periodic array of flux tubes. The two approaches differ in a number of other respects as well.

4. The CLV of the Fe I 5250.22Å Stokes V area asymmetry

In the following we describe six steps taken to isolate the influence of various components of the standard model – described in Sect. 2 – on the CLV of the Stokes V asymmetry. In steps 1 to 4, models that are only fragments of the standard model are considered. In particular these models may have unphysical flow fields. In all these cases the non-magnetic atmosphere has the modified HSRASP temperature profile $T^* = T_{HSRASP} - 300$ K. Only the models used in steps 5 and 6 include all the components of the standard model. For these tests we only consider Fe I 5250.22 Å, and postpone the discussion of another line to the next section.

1. As the aspect angle θ is changed, so is the angle between the line of sight and the magnetic field, so that the π–component of the line becomes more prominent near the limb. Auer & Heasley (1978) have shown that, together with a velocity gradient, this effect produces a centre-to-limb variation of the Stokes V asymmetry. To test the importance of this effect we first calculated the CLV using the model described in Sect. 2, but with only pure vertical downflows in the surroundings of the flux tubes, chosen such that the observed δA at disc centre is reproduced. This model completely fails to reproduce the observed CLV of δA. The calculated δA remains strictly positive and actually increases towards the limb, since in this configuration contributions to δA of the same signature are produced at all magnetic/non-magnetic boundaries, the number of which increases towards the limb along any single ray.

2. While observations at disc centre are only sensitive to the *vertical* component of the velocity field, its *horizontal* component becomes relevant for observations closer to the limb. Schüssler (1990) proposed that this is the main mechanism giving rise to the change in sign of δA. However, Fig. 1 illustrates that the two points at which a typical inclined ray intersects the flux-tube boundary give opposite contributions to δA. In this step we therefore consider a purely horizontal flow in the non-magnetic surroundings of the tubes, directed toward the flux-tube axis. Of course, $\delta A = 0$ at $\mu = 1$, since no vertical flow is present. At the limb δA is small but positive in our calculations. We therefore conclude that the presence of a horizontal inflow by itself is not sufficient to produce the observed sign reversal, although it later turns out to be a necessary ingredient (within the confines of the standard model).

3. In a third step we have combined an inflow with a downflow, as illustrated in Fig. 2. Although the observations at disc centre may now be reproduced, the asymmetry does not change sign near the limb, similar to step (2).

4. Next an upflow has been introduced, leading to a model of the type shown in Fig. 4, left. This model, finally, reproduces the observed (positive) δA at disc centre, and, at the same time,

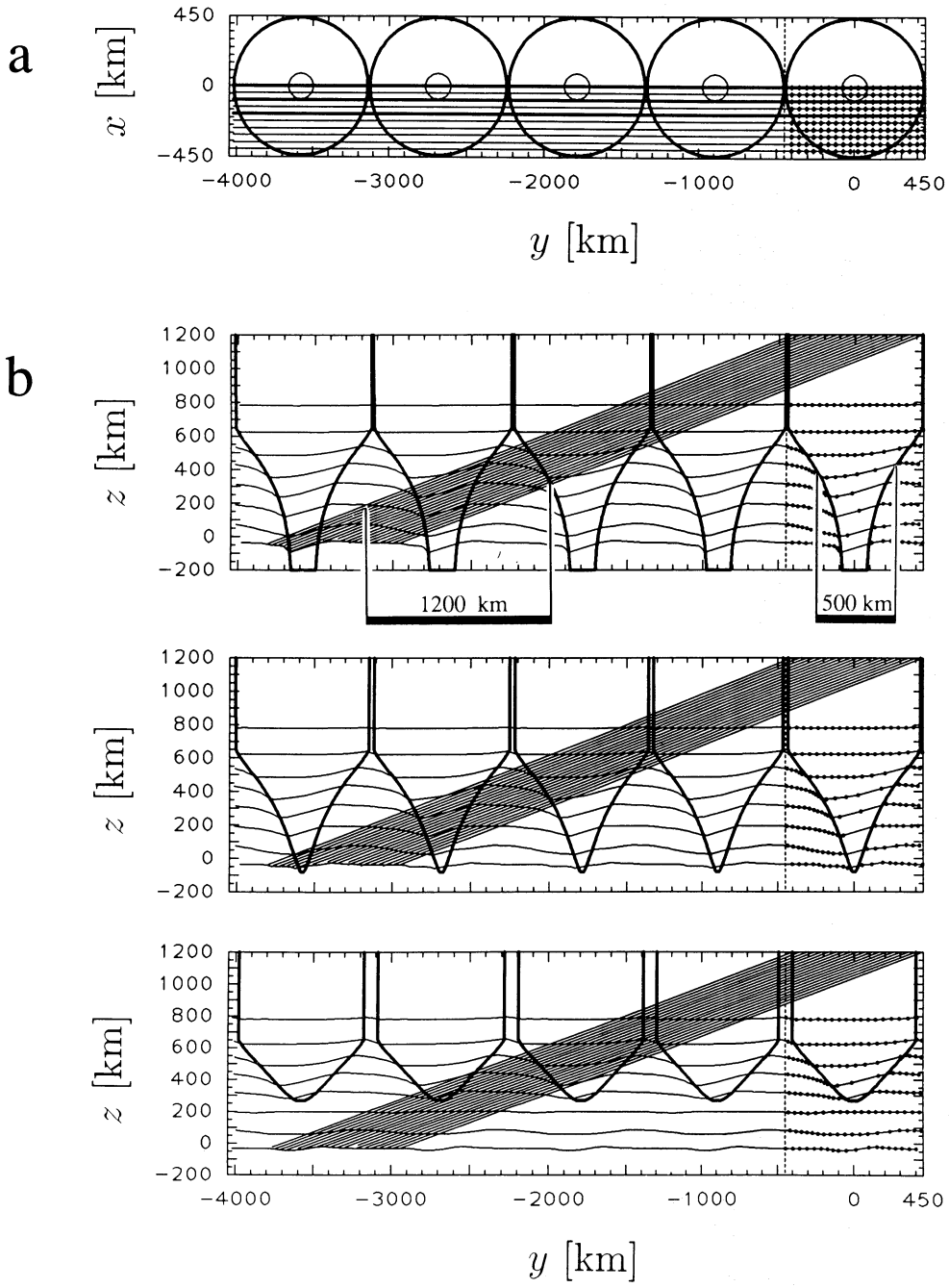

Fig. 5. Illustration of the model geometry for Stokes V calculations near the limb. **a.** An array of merged flux tubes as seen from above (thick circles). Each horizontal line indicates the position of a vertical plane cutting the model. Each point to the right is the entry point into the top of the model of a ray lying in one of the vertical planes. **b.** Illustration of the three vertical sections that are indicated in Fig. 5a by the thick horizontal lines. The first frame represents the plane of symmetry (upper thick line in Fig. 5a), the middle and bottom frames correspond to the middle and lowest heavy lines in Fig. 5a, respectively. The rays, along which the radiative transfer is calculated, enter the model from the top under an aspect angle of $\theta = 70°$ to the vertical ($\mu = \cos\theta = 0.34$) for simulation of a low resolution observation close to the limb. The thick lines are the contours where the flux-tube surfaces intersect with the vertical planes. The thin horizontally running curves are sections through surfaces of equal optical depth τ_c as "seen" under an aspect angle $\theta = 70°$), in steps of $\Delta \log \tau_c = 1$ from $\log \tau_c = -6.0$ to +1.0. For a spectral line which is formed in the layer $-3 \lesssim \log \tau_c \lesssim -1$ the horizontal range affecting Stokes V on both sides of a given flux tube is indicated below the first frame, for observations near the limb (left) and at disc centre (right)

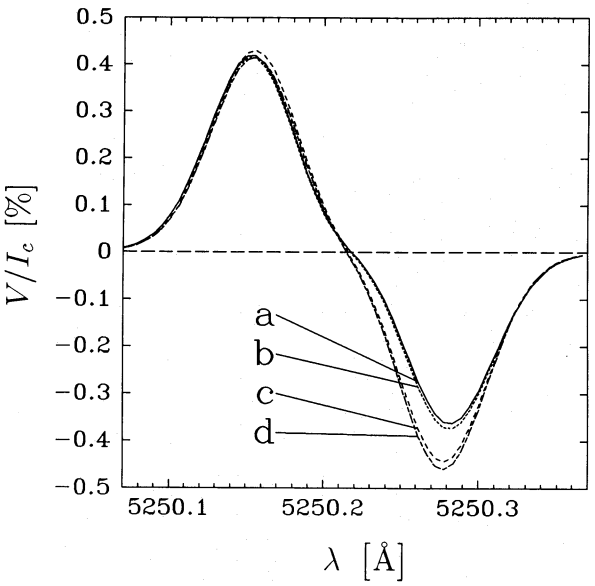

Fig. 6. Stokes V profiles of Fe I 5250.22 Å at $\theta = 70°$ ($\mu = 0.34$) arising from an array of flux tubes as shown in Fig. 5. The profiles correspond to models with different velocity fields (Sect. 4). Curve a: inflow and downflow without any upflow (step 3); curve b: upflow instead of inflow in the outer parts of the model (step 4), curve c: like curve b, but including a temperature-velocity correlation (step 5), curve d: like curve c, but with enhanced horizontal velocity components (step 6)

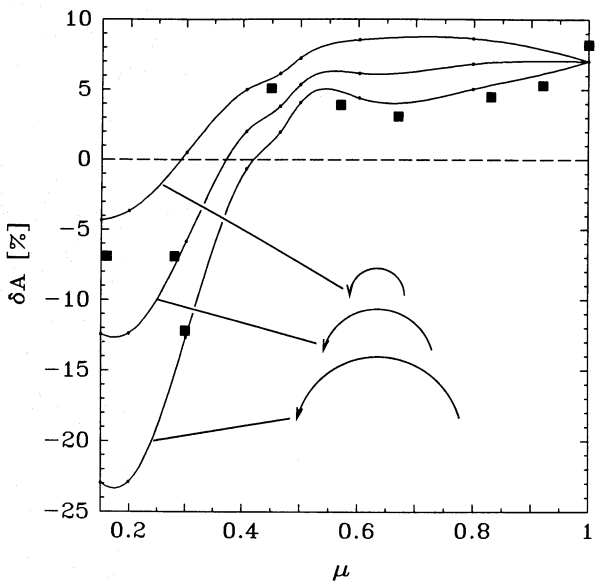

Fig. 7. Observed (squares) and calculated (curves) centre-to-limb variation of the relative area asymmetry of Stokes V profiles of Fe I 5250.22 Å. The models include a cool downflow near the flux-tube boundaries and a warm upflow further away from them (steps 5 and 6). They differ only in the radial velocity components as indicated by the arrows. The uppermost curve results for suppressed, the lowest curve for enhanced radial velocities with respect to the standard model (middle curve)

yields a negative δA near the limb. However, δA changes sign only very close to the limb (at $\mu \approx 0.2$) and never drops below -1% to -2% for $\mu \gtrsim 0.1$, whereas observations show the sign reversal at $\mu \approx 0.4$ and values of -5% to -10% for $0.1 \leq \mu \leq 0.3$. Apparently some important ingredient is still missing in the model.

5. In this step, a temperature-velocity-correlation of the type described by Eq. (7), i.e., a warm upflow and a cool downflow, has been added. This model is able to produce both a large positive δA at $\mu = 1$ and a large negative δA for small values of μ. To test which is more important, the upflow or the fact that the temperature structure of the non-magnetic atmosphere is inhomogeneous, we have changed the inflow–downflow model of step (3) in the sense that the downflow remains cool, whereas the purely inflowing part of the atmosphere is heated by 1000 K at equal geometrical height. This model leads to an equally pronounced negative δA near the limb, confirming that the temperature inhomogeneity is more important than the upflow. However, an upflow is required in order to conserve mass, so that all the following models incorporate it.

6. Finally, the behaviour of the asymmetry can be considerably influenced by changing the ratio of the maximum horizontal velocity to the maximum vertical velocity component. Enhanced horizontal velocities result in more pronounced negative values of δA near the limb but only as long as the temperature and velocity are correlated as in step 5.

The effect on the line profile of some of the steps described above are illustrated in Fig. 6, which shows calculated Stokes V profiles of the line Fe I 5250.22 Å at $\mu = 0.34$, i.e., at an angle $\theta = 70°$. At this position on the solar disc (close to the limb) the area asymmetry of the *observed* Stokes V profile has already changed sign, i.e., the red wing dominates the blue. The synthetic profiles in Fig. 6 all result from the same magnetic field configuration but from different velocity fields in the field-free atmosphere between the flux tubes. Curve (a) represents the results from step 3, curve (b) corresponds to step 4, curve (c) to step 5 (where in comparison to step 4 a temperature-velocity correlation has been introduced), and curve (d) shows the effect of arbitrarily enhancing the horizontal velocities by a factor of two while leaving the vertical components and the associated temperature structures unchanged (step 6). Note that the profiles shown in Fig. 6 have been convolved with a macro-turbulence of 2 km/s. This is responsible for the small shift in the zero-crossing wavelength of some of the profiles (Solanki & Stenflo 1986).

Having identified some of the main parameters controlling the CLV and the sign reversal of δA, we have compared the synthetic profiles with the observations. Only the results of steps 5 and 6 are discussed further. Figure 7 shows the observed (squares, data taken from Stenflo et al. 1987) and calculated relative area asymmetry of the Stokes V profiles of the Fe I 5250.22 Å line as a function of $\mu = \cos\theta$. The middle curve corresponds to the $\delta A(\mu)$ produced with the model of step 5. The maximum horizontal inflow is 2.9 km/s, the maximum vertical velocity is 3.8 km/s. The ΔT parameter of Eq. (3) is chosen to be 1000 K. The lowest curve results when the horizontal velocity component is arbitrarily enhanced by a factor of 2, while

the uppermost curve is obtained if the horizontal velocity is reduced by the same factor. The correspondence between these models and the observations is gratifying.

Before considering the dependence of δA on the free parameters of the model in detail, let us consider the basic causes of the area asymmetry and of its sign reversal. As noted in Sect. 1 (Fig. 1) it is not a priori obvious whether the standard configuration will or will not produce a sign reversal. The series of test calculations described so far have shown that three main ingredients are required to obtain the correct qualitative $\delta A(\mu)$ dependence:

1. A downflow near the flux tube. This is needed to obtain $\delta A > 0$ at disc centre. As illustrated in Fig. 5b, at $\mu \approx 1$ only the flow close to the flux-tube boundary gives a significant contribution to δA.
2. An inflow somewhat further away from the tube. This is a necessary ingredient to obtain a reversal in sign of δA, but is not by itself sufficient. This can be easily seen by considering Fig. 1 again. For an inclined line-of-sight the longitudinal velocity on the discward side of the flux tube is always larger than the longitudinal velocity on the limbward side. Thus, obviously, except for the unlikely case that the velocities are much larger than the line widths (Grossmann-Doerth et al. 1989), δA will remain strictly positive, except possibly at $\mu = 0$, where $\delta A = 0$. This implies the need for another factor which gives additional weight to the flow on the limbward side of the tube.
3. The temperature-velocity correlation appears to be this missing factor. We suspect it to be mainly responsible for the change in sign of δA by its effect on the continuum. Since the magnitude of the horizontal velocity decreases with height [Eq. (6)] rays which see the largest longitudinal velocity on the discward side of the flux tube intersect $\tau_c = 1$ either inside the flux tube or just outside the limbward tube boundary in the cool downflow lane and are therefore weighted by a low continuum intensity. The rays which see a large longitudinal velocity on the limbward side, on the other hand, have a good likelihood of reaching $\tau_c = 1$ further away from the flux tube, at a position at which the continuum intensity is large, thus giving it a larger weight. Very close to the limb, as $\mu \longrightarrow 0$, this explanation no longer works and we expect the asymmetry to approach zero.

5. Results of a parametric survey

We have analysed the influence of the free model parameters on the CLV of the Stokes V area asymmetry by calculating a series of 35 models. For each model the Stokes profiles of Fe I 5250.2 Å and the profiles of Fe I 5083.3 Å, a stronger line with a larger measured δA, are calculated at $n_\mu = 9$ disc positions. Each model has 7 free parameters in all: filling factor, flux-tube radius, ratio of area with upflowing to the area with downflowing gas, the temperature contrast between upflow and downflow, the height at which v_r is largest [$\bar{z}$ in Eq. (6)], and finally, the exponents m and n which determine the shape of the $v_r(z)$ curve [see Eq. (6) and Fig. 3]. It is obvious that the present parametric survey can sample the seven dimensional parameter space only partially. Improving the sampling significantly runs into practical problems of computing time: Even the restricted parametric survey presented here involves the computation of over 10^5 Stokes line profiles.

The influence of the different parameters on the CLV of δA is complex. For example, the area ratio between the upflow and downflow regions has only a minute influence on δA for flux tubes with diameter $\lesssim 250$ km, but it has a large influence for flux tubes with a diameter of, e.g., 400 km. However, we stress that the models show one robust property in agreement with the observations: δA is positive near the centre of the solar disc and changes sign as μ decreases. Although we covered a relatively large range of parameters we found only one single model (with exception of the non-standard models discussed in Sect. 4) which did not exhibit this behaviour. Thus, this basic observational fact is generally reproduced by the standard model. This suggests that the standard model has all the main ingredients to *qualitatively* reproduce the data. On the whole we find that all the model parameters have a significant effect, with the possible exception of the filling factor α, which leaves the shapes of the $\delta A(\mu)$ curves relatively unaffected and only shifts their zero-crossing point to slightly larger values of μ with increasing filling factor.

Interestingly, δA does not continue to become increasingly more negative as μ keeps decreasing. Practically all models show signs of a flattening in the $\delta A(\mu)$ curves near the limb and quite a few suggest that $|\delta A|$ begins to decrease again for $\mu \lesssim 0.2 - 0.3$. For 2 models δA of 5083.3 Å actually becomes slightly positive again at $\mu \lesssim 0.2$. We expect that at $\mu = 0$ the δA produced by our model to be zero, or negligibly small. Therefore the flattening of the $\delta A(\mu)$ curves and the decrease of $|\delta A|$ for very small μ is not unexpected.

The velocity field is mainly determined by the $v_r(z)$ profile, to be prescribed at the interface of the upflow and the downflow region. The characteristics of the $v_r(z)$ profile, namely its shape (parameter n) and the vertical position of its peak (parameter $\bar{z}$) has a large influence on $\delta A(\mu)$. The CLV curves shown in Fig. 8 differ by the shape, i.e., the value of n. As n is decreased from 9 (the standard value) to 6, which leads to radial velocities reaching farther up in the atmosphere (cf. Fig. 3), the δA values are generally increased (uppermost curve). The increase of v_r at greater height leads to an increase in v_z there as well. If this effect is artificially suppressed (by an arbitrary reduction of the v_z-component to about the values of the $n = 9$ model) the lowest curve results. In each of these cases the maximum of the absolute value of the radial velocity lies at $\bar{z} = 0$ km. If we vary $\bar{z}$ slightly and keep $n = 9$ fixed, we obtain Fig. 9. The three curves correspond to $\bar{z} = 0$, -50 km, and +50 km ($\bar{z}$ is measured with respect to $\tau_{5000} = 1$ in the modified HSRASP atmosphere). Again, the effect on the CLV curves is considerable, indicating a great sensitivity of the CLV of δA on the details of the overshooting convective motion in the line forming layers of the atmosphere. The Fe I 5083 Å line behaves similar.

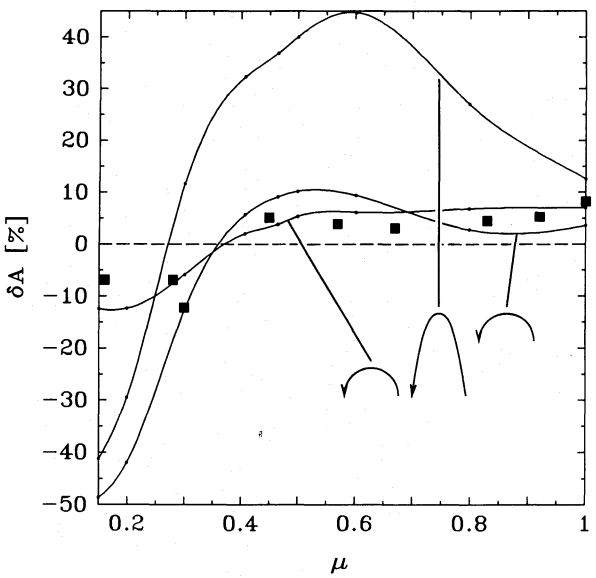

Fig. 8. The CLV of the area asymmetry of the Fe I 5250.2 Å Stokes V profile. The three curves differ in the shape of the prescribed radial velocity profile [Eq. (6)]. In the standard case $n = 9$ (corresponding to the overturning arrow on the left). The uppermost curve results for $n = 6$, i.e., for motions with a pronounced overshoot that reaches farther up in the atmosphere (symbolized by the overturning arrow in the middle). The remaining curve results for $n = 6$ and suppressed vertical velocities (overturning arrow on the right)

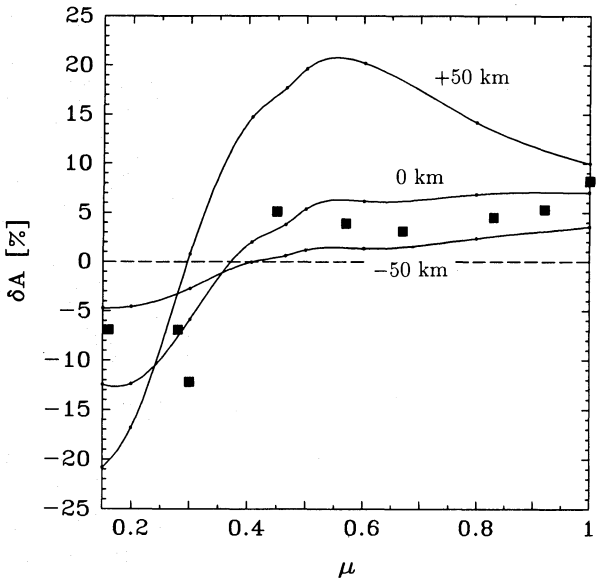

Fig. 9. The CLV of the area asymmetry of the Fe I 5250.2 Å Stokes V profile. The three curves differ in the height $\bar{z}$ at which the maximum radial velocity of the external flow occurs [Eq. (6)]. The values of $\bar{z}$ are given in km with respect to $z = 0$ of the model

As a next example we plot in Fig. 10 the CLV of δA of the Fe I 5083 line for three models with different flux-tube diameters: 100 km, 200 km, and 400 km keeping the filling factor constant at $\alpha = 0.05$. The solid curves refer to models in which, at the height $z = 0$, the downflow is confined within a ring around the flux tube of constant thickness of 120 km. Interestingly, the CLV changes drastically near disc centre, disfavouring the smallest tube when compared with observations.

If the ratio of the radial extent of the downflow to the upflow is kept constant at 0.53 (the value of the original standard model) the dotted curves result. Note that the asymmetry of the large tube no longer changes sign towards the limb but, on the contrary, shows increasingly positive δA values there. This is the only model of our sample which shows such a behaviour.

We find that the two lines generally behave in a qualitatively similar manner. However, there are considerable quantitative differences. The same model usually produces up to a factor of 2 larger δA values (both negative and positive) for the 5083.3 Å line compared to the 5250.2 Å line. In addition, the shapes of the $\delta A(\mu)$ curves are usually somewhat different: those of the Fe I 5083.3 Å line have a positive hump around $\mu = 0.5 - 0.6$ in the majority of the models. No such hump is present in the observations. Thus, only very few models give $\delta A(\mu)$ curves of the 5083.3 Å line which resemble the observations even vaguely (an example is the curve for the flux tube with a diameter of 400 km in Fig. 10). To us this suggests that, although the basic structure of our model is correct, its details still require considerable improvement.

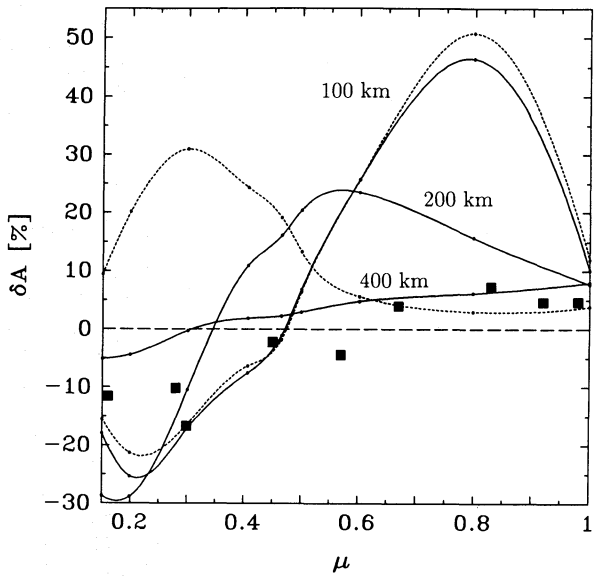

Fig. 10. The CLV of the area asymmetry of the Fe I 5083.3 Å Stokes V profile. The three solid curves refer to models with different diameters at $z = 0$ (values given in the frame), but with a constant thickness of the downflow region. If the ratio of the radial extent of the downflow to the upflow region is kept constant, the dotted curves result

6. Conclusions

We have investigated the centre-to-limb variation of the area asymmetry of synthetic Stokes V line profiles. The underlying hydromagnetic model consists of a cluster of rotationally symmetric magnetic flux tubes surrounded by non-magnetic plasma in stationary motion that resembles a granular flow pattern. From

a parametric survey, in which mainly the velocity field was varied, we come to the following conclusions:

1. The model of magnetic flux tubes embedded in the downflow lanes of granules produces an inversion of the sign of the area asymmetry of Stokes V profiles for a very wide range of parameters. This is one of the most robust features of this model.
2. The centre-to-limb variation of the area asymmetry of Stokes V profiles can be used as a sensitive tool for investigating the velocity and temperature structure of the granulation in solar active regions.
3. The closer the assumed non-magnetic atmospheric dynamics (in the environment of the flux tubes) correspond to the solar granulation (i.e., warm central upflows, horizontal velocities, and cool downflows), the better the observed centre-to-limb behaviour of the Stokes V asymmetry δA is reproduced. The temperature-velocity-correlation of granular convective motions is an essential ingredient for reproducing the observed δA away from disc centre. This is a sign that the basic picture of magnetic flux tubes and of their relation to the surrounding gas, as outlined in Sect. 1, is correct.
4. Velocity fields in the *non-magnetic* environment are able to quantitatively reproduce not only the observed Stokes V area asymmetry (δA) of Fe I 5250.22 Å at disc centre, but also its centre-to-limb variation, including the sign reversal of the asymmetry around $\mu = 0.4$ ($\theta \simeq 60°$). The δA of Fe I 5083.3 Å, a stronger line, can also be qualitatively reproduced, but we were unable to find any model, within our limited set of calculations, which can simultaneously reproduce the CLV of the δA of both lines in a quantitative manner. This suggests that some important feature is still missing in the models.
5. The calculated line profiles do not show any shift of the zero-crossing wavelength at any position on the disc (as long as no macro-turbulence is introduced), in agreement with the observations of Stenflo et al. (1987), Pantellini et al. (1988), and Wiehr (1987, private communication). This is a direct result of the fact that the present models do not include any velocity within the magnetic features. As proved by Grossmann–Doerth et al. (1988, 1989), such a segregation of velocity and magnetic fields always leaves the zero-crossing wavelength of the V profiles unshifted, irrespective of the geometrical details. However, we do foresee possible problems for mechanisms which make use of velocities within the flux tubes to produce a non-zero δA and rely on special geometries to keep the zero-crossing shift small (e.g. Sánchez Almeida et al. 1988, 1989, and 1990), since the geometry of the field and of the velocity along the line of sight is strongly dependent on θ. For example, near disc centre the main contribution to the Stokes V signal comes from rays which remain completely within the magnetic features (Solanki 1989), whereas near the limb every ray passes at least partially through the non-magnetic atmosphere (cf. Fig. 5).
6. The modelled "granular" flows also produce an asymmetry, δa, between the amplitudes of the Stokes V profiles. The synthetic δa values generally follow the δA values relatively closely, while the observed δa values are in general more positive. Thus the observed δa of most Fe I lines barely changes sign near the limb (Pantellini et al. 1988) whereas the synthetic δa become strongly negative. Following Solanki (1989) we conclude that an additional source for the amplitude asymmetry, probably a velocity within the flux tubes, is required. Since $\delta a_{\rm synth} < \delta a_{\rm obs}$ at all θ–values the missing velocity must have both a vertical and horizontal component. For the vertical component nonlinear waves (Grossmann-Doerth et al. 1991) and siphon flows (Degenhardt & Kneer 1992) have been proposed. The nature of the horizontal velocity component within the flux tubes is still unclear. To explain excess, non-thermal, non-magnetic widths of Stokes V profiles, Pantellini et al. (1988) proposed the presence of kink mode and torsional Alfvén mode waves in small flux tubes. These, and horizontal flux-tube motions (due to buffeting by the granulation), appear to be the main contenders for changing the δa near the limb as well.

Finally, let us consider possible improvements for the future. One major shortcoming of the present model is the too simple representation of granulation. Examples of model components which are missing in the present contribution are: a) the inversion of the temperature-velocity correlation in the upper half of the photosphere (Stein & Nordlund 1989, Karpinsky 1990), b) localized high velocities (i.e., supersonic velocities and the associated shocks, e.g. Cattaneo et al. 1990, Malagoli et al. 1990, Steffen & Freytag 1991), c) a more realistic geometry of the granulation. The inclination of the flux tubes may also be of relevance. Solanki et al. (1987) showed that for a number of observed regions the flux tubes were inclined to the vertical by more than 10°. It does not appear to be feasible to overburden the present model by introducing these additional components, particularly since then the already large number of free parameters will increase further. Progress in this field will have to await self-consistent models of granulation in the presence of small magnetic flux tubes.

Acknowledgements. We thank J.O. Stenflo for helpful discussions and a careful reading of the manuscript. The work of one of us (M.B.) has been supported by grant No. 20–31 289.91 of the Swiss National Science Foundation. O.S. wishes to acknowledge financial support by the Deutsche Forschungsgemeinschaft under grant SCHU 500/6-1.

References

Audic, S.: 1991, *Solar Phys.* **135**, 275
Auer, L.H., Heasley, J.N.: 1978, *Astron. Astrophys.* **64**, 67
Beckers, J.M.: 1969a, *Solar Phys.* **9**, 372
Beckers, J.M.: 1969b, *Solar Phys.* **10**, 262
Bünte, M.: 1989, *Diplomarbeit*, ETH Zürich
Bünte, M., Steiner, O., Solanki, S.K.: 1991, in *Solar Polarimetry* L. November (ed.), National Solar Observatory, Sacramento Peak, NM, p.468
Cattaneo, F., Hurlburt, N.E., Toomre, J.: 1990, *Astrophys. J.* **349**, L63
Chapman, G.A.: 1979, *Astrophys. J.* **232**, 923
Degenhardt, D., Kneer, F.: 1992, *Astron. Astrophys.* **260**, 411

Deinzer, W., Hensler, G., Schüssler, M., Weisshaar, E.: 1984, *Astron. Astrophys.* **139**, 435
De Martino, S.: 1986, *Diplomarbeit*, ETH Zürich
Gingerich, O., Noyes, R.W., Kalkofen, W., Cuny, Y.: 1971, *Solar Phys.* **18**, 347
Grossmann–Doerth, U., Schüssler, M., Solanki, S.K.: 1988, *Astron. Astrophys.* **206**, L37
Grossmann–Doerth, U., Schüssler, M., Solanki, S.K.: 1989, *Astron. Astrophys.* **221**, 338
Grossmann–Doerth, U., Schüssler, M., Solanki, S.K.: 1991, *Astron. Astrophys.* **249**, 239
Gustafsson, B.: 1973, *Uppsala Astron. Obs. Ann.* **5**, No. 6
Illing, R.M.E., Landman, D.A., Mickey, D.L.: 1975, *Astron. Astrophys.* **41**, 183
Karpinsky, V.N.: 1990, in *Solar Photosphere: Structure, Convection, and Magnetic Fields*, J.O. Stenflo (ed.), Kluwer, Dordrecht, IAU Symp. **138**, 67
Knölker, M., Grossmann-Doerth, U., Schüssler, M., Weisshaar, E.: 1991, *Adv. Space Res.* **11**, (5)285
Malagoli, A., Cattaneo, F., Brumell, N.H.: 1990, *Astrophys. J.* **361**, L33
Nordlund, Å.: 1985, in *Theoretical Problems in High Resolution Solar Physics*, H.U. Schmidt (ed.), Max Planck Inst. f. Astrophys., München, p.1
Nordlund, Å.: 1986, in *Small Scale Magnetic Flux Concentrations in the Solar Photosphere*, W. Deinzer et al., (eds.), Vandenhoeck and Ruprecht, Göttingen, p. 83
Pantellini, F.G.E., Solanki, S.K., Stenflo, J.O.: 1988, *Astron. Astrophys.* **189**, 263
Ringenbach, A.: 1987, *Diplomarbeit*, ETH Zürich
Sánchez Almeida, J., Collados, M., Del Toro Iniesta, J.C.: 1988, *Astron. Astrophys.* **201**, L37
Sánchez Almeida, J., Collados, M., Del Toro Iniesta, J.C.: 1989, *Astron. Astrophys.* **222**, 311
Sánchez Almeida, J., Collados, M., Del Toro Iniesta, J.C.: 1990, *Astrophys. Space Sci.* **170**, 31
Schüssler, M.: 1990, in *Solar Photosphere: Structure, Convection, and Magnetic Fields*, J.O. Stenflo (ed.), Kluwer, Dordrecht, IAU Symp. **138**, 161
Schüssler, M.: 1992, in *The Sun – a Laboratory for Astrophysics*, J. T. Schmelz and J. C. Brown (ed.), NATO Advanced Study Institute, Kluwer, Dordrecht, in press
Solanki, S.K.: 1986, *Astron. Astrophys.* **168**, 311
Solanki, S.K.: 1987, Ph.D. Thesis, ETH Zürich
Solanki, S.K.: 1989, *Astron. Astrophys.* **224**, 225
Solanki, S.K.: 1992, *Space sci. Rev.*, in press
Solanki, S.K., Pahlke, K.D.: 1988, *Astron. Astrophys.* **201**, 143
Solanki, S.K., Stenflo, J.O.: 1984, *Astron. Astrophys.* **140**, 185
Solanki, S.K., Stenflo, J.O.: 1985, *Astron. Astrophys.* **148**, 123
Solanki, S.K., Stenflo, J.O.: 1986, *Astron. Astrophys.* **170**, 120
Solanki, S.K., Keller, C., Stenflo, J.O.: 1987, *Astron. Astrophys.* **188**, 183
Spruit, H.C.: 1974, *Solar Phys.* **34**, 277
Steffen, M.: 1990, in *Stellar Atmospheres: Beyond Classical Models*, L. Crivellari and I. Hubeny (eds.), Kluwer, Dordrecht, p. 247
Steffen, M., Freytag, B.: 1991, *Reviews of Modern Astron.* **4**, p. 43
Steffen, M., Ludwig, H.–G., Krüß, A.: 1989, *Astron. Astrophys.* **213**, 371
Stein, R.F., Nordlund, Å.: 1989, *Astrophys. J.* **342**, L95–98
Steiner, O.: 1992, in *Infrared Solar Physics*, D. Rabin (ed.), Kluwer, Dordrecht, IAU Symp. **154**, in press
Steiner, O., Pneuman, G.W., Stenflo, J.O.: 1986, *Astron. Astrophys.* **170**, 126
Stenflo, J.O.: 1976 in *Basic Mechanisms of Solar Activity*, V. Bumba and J. Kleczek (eds.), Reidel, Dordrecht, IAU Symp. **71**, 69
Stenflo, J.O.: 1989, *Astron. Astrophys. Rev.* **1**, 3
Stenflo, J.O., Harvey, J.W.: 1985, *Solar Phys.* **95**, 99
Stenflo, J.O., Harvey, J.W., Brault, J.W., Solanki, S.K.: 1984, *Astron. Astrophys.* **131**, 33
Stenflo, J.O., Solanki, S.K., Harvey, J.W.: 1987, *Astron. Astrophys.* **171**, 305
Title, A.M., Tarbell, T.D., Topka, K.P.: 1987, *Astrophys. J.* **317**, 892
Van Ballegooijen, A.A.: 1985, in *Theoretical Problems in High Resolution Solar Physics*, H.U. Schmidt (ed.), Max Planck Inst. f. Astrophys., München, p.177
Walton, S.R.: 1987, *Astrophys. J.* **312**, 909
Wiehr, E.: 1985, *Astron. Astrophys.* **149**, 217
Wiehr, E.: 1987, in *Cool Stars, Stellar Systems, and the Sun*, J.L. Linsky and R.E. Stencel (eds.), Lecture Notes in Physics Vol. 291, Springer Verlag, Berlin, p.54
Zayer, I., Solanki, S.K., Stenflo, J.O.: 1989, *Astron. Astrophys.* **211**, 463

This article was processed by the author using Springer-Verlag TEX A&A macro package 1992.